ACS Macro Letters

pubs.acs.org/macroletters Letter

Symmetry-Broken Patches on Gold Nanoparticles through Deficient Ligand Exchange

Hanyi Duan, Qiang Luo, Zichao Wei, Yao Lin,* and Jie He*

Cite This: ACS Macro Lett. 2021, 10, 786−790 Read Online

ACCESS | Metrics & More | Article Recommendations | Supporting Information

ABSTRACT: Symmetry-broken nanoparticles (NPs) are important building blocks with directional interparticle interaction as a key to access the precise organization of NPs macroscopically. We report a facile, one-pot synthetic approach to prepare high-quality symmetry-broken plasmonic gold NPs (AuNPs). Symmetry-broken patterning is achieved through deficient ligand exchange of isotropic AuNPs with thiol-terminated polystyrene (PS-SH) in the presence of an amphiphilic polymer surfactant. The concentration of PS-SH plays a dominant role in tuning surface patterning and coverage of AuNPs. The formation of asymmetric surface patches arises from the interplay between the conformational entropy of polymer ligands and the interfacial energy between polymer-grafted AuNPs and the solvent. Our method illustrates new paradises to design asymmetric NPs with directional interparticle interactions to access the precise organization of NPs.

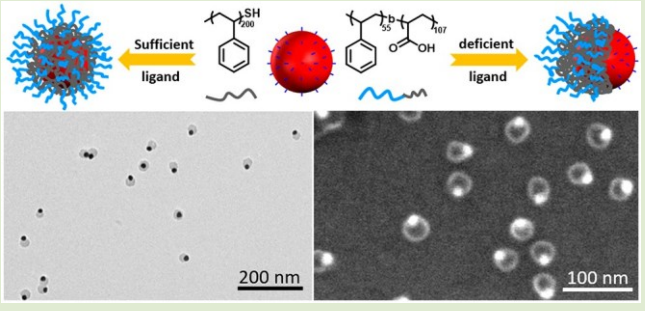

Polymer-grafted plasmonic nanoparticles (PGPNs) consisting of a plasmonic nanoparticle (NP) core chemically grafted with polymer tethers have received continuous attention as part of functional polymer nanocomposites over the past decade.[1] Polymers as surface ligands that dominate the interparticle interaction direct the organization of plasmonic NPs macroscopically to control their ensemble properties, such as tunable plasmonic properties of PGPNs.[1a,2] For example, PGPNs with amphiphilic mixed polymer tethers[3] or block copolymers (BCPs)[4] can assemble into abundant nanostructures with promising applications in nanomedicine,[5] sensing,[6] and catalysis.[7] While those assemblies are interesting, the self-assembly mechanism usually involves the symmetry-broken rearrangement of polymer ligands.[8] In many cases, such broken symmetry plays a key role in creating directional interaction of plasmonic NPs and thus the formation of sophisticated assemblies.[9] The symmetry-broken arrangement of polymers can be done through two strategies, including site-specific grafting and phase segregation.[10] Site-specific binding relies on the recognition of the surface energy difference among, for example, different facets[2b,11] and corner or edge sites of plasmonic NPs.[10b,12] It usually applies to anisotropic plasmonic NPs with distinct binding sites on the surface. On the other hand, phase segregation driven by the thermodynamically unfavorable mixing of ligands can pattern plasmonic NPs, even with isotropic surface properties.[13] Ligands with different lengths and hydrophobicity have been demonstrated to form surface patterns, like Janus-type segregation[13a,14] and strips,[15] on NPs.

More recently, polymer ligands have been reported to show very similar hydrophobicity-driven surface patterning on plasmonic NPs. PGPNs with hydrophobic polymer ligands, for example, thiol-terminated polystyrene (PS-SH), undergo unique phase segregation when transferred from a good to a poor solvent.[8b,16] As chemically linked to plasmonic NPs, hydrophobic PS-SH when collapsed can segregate to form patches on plasmonic NPs instead of symmetric core−shell coating. Although those surface patches of isotropic plasmonic NPs are interesting, the preparation condition is extremely delicate, for example, at extremely low concentrations to avoid interparticle interactions. The other key challenge in hydrophobicity-driven surface patterning of PGPNs is to control the low grafting density of PS-SH while balancing their colloidal stability during ligand exchange.[8b] In this Letter, we propose to limit the grafting density of PS-SH simply through continuously reducing the concentration of PS-SH ($C_{PS\text{-}SH}$), namely, deficient ligand exchange (DLE). To address the stability of PGPNs, concurrently adding an amphiphilic BCP surfactant, like poly(acrylic acid)-block-polystyrene (PAA-b-PS), can protect the PS patches to avoid interparticle interaction. Herein, a new "one-pot" DLE approach is reported

Received: April 14, 2021
Accepted: June 7, 2021
Published: June 9, 2021

https://doi.org/10.1021/acsmacrolett.1c00252
ACS Macro Lett. 2021, 10, 786−790

to rationally design surface patterning on spherical gold NPs (AuNPs). Our synthetic approach is summarized in Figure 1a.

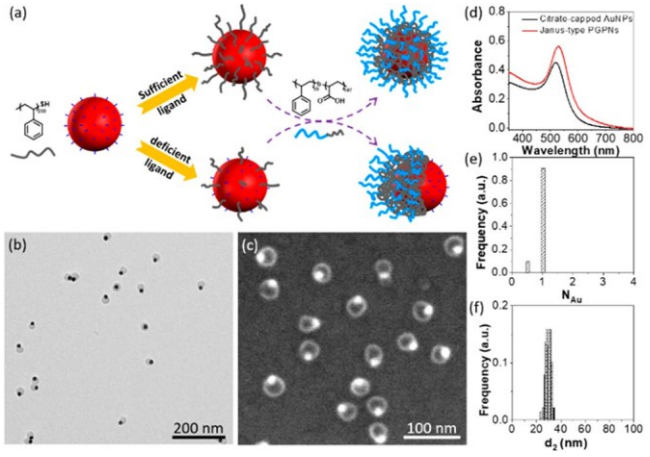

Figure 1. (a) Surface patterning of AuNPs: core−shell (up) and Janus-type (down) PGPNs. (b) TEM and (c) SEM of Janus-type PGPNs. (d) UV−vis of citrate-capped AuNPs and Janus-type PGPNs in water. Histogram of (e) N_{Au} and (f) diameter (d_2) averaged from >200 NPs.

In the mixture of PS-SH, PAA-b-PS, and AuNPs, the surface of AuNPs is fully coated with brush-like polymers in the presence of sufficient PS-SH; thus, core−shell nanostructures uniformly coated with polymers are observed in a poor solvent of PS. When reducing $C_{PS\text{-}SH}$, a clear morphological transition from core−shell to Janus-type PGPNs is observed. Our key findings are 3-fold. First of all, we resolve the synthetic challenges in colloidal stability of asymmetric NPs prepared through hydrophobicity-driven surface patterning. Hydrophobic polymer ligands (either homopolymer[8b] or BCP[16b,17]) show strong interparticle interactions, particularly in water. The addition of a nonbound BCP surfactant endows water solubility of as-resultant Janus NPs with a concentration of >10 mg/mL. Second, the surface patterning of plasmonic NPs is achieved solely by varying the concentration of PS-SH. Without the interfacing from other ligands, the use of single polymer ligands simplifies the symmetry-broken patterning of AuNPs. We tackle the long-standing issue to control the ligand density of polymers, especially in the low grafting density region, while retaining their solubility. The surface grafting density of hydrophobic PS ligands is clearly identified to control the surface patterning. Third, control of the surface coverage of AuNPs and polymer domain size is showed by varying the concentration and molecular weights (M_w) of PS-SH. It makes our method simple, general, and highly reproducible. We expect that it opens new doors to design symmetry-broken PGPNs as unique building blocks for their hierarchical self-assembly.[18]

To prepare Janus-type PGPNs, 0.45 mg of PS_{200}-SH (M_w = 20.8 kg/mol, Đ = 1.08, and 0.9 μM) and 20 mg of PAA_{107}-b-PS_{55} (M_w = 13.6 kg/mol, Đ = 1.2, and 73.5 μM) were first dissolved in 20 mL of dimethylformamide (DMF). Then, 0.2 mL of preconcentrated citrate-capped AuNPs (13.1 ± 1.2 nm, 5.2 mg, see SI for details) was added dropwise to the DMF solution of the two polymers. After sonication for 1 min, the mixture was incubated overnight to ensure polymer grafting on AuNPs. Afterward, 3.6 mL of water (16 vol % of the final solution) was added to the mixture, and the solution became turbid immediately since water is a nonsolvent for PS. The mixture was then annealed at 100 °C for 1 h. The solution was subsequently cooled down slowly with a cooling rate of approximately 10 °C per 1 h. The slow cooling process allowed the rearrangement of polymer chains to form more uniform nanostructure. After the self-assembly was quenched with excess water, as-resultant PGPNs were collected by centrifugation (see SI for details). Figure 1b shows the representative transmission electron microscope (TEM) image of Janus-type PGPNs. The morphological asymmetry of Janus-type PGPNs can be visualized by the electron density contrast under TEM where dense Au domains (Figure S1) are darker and spherical polymer domains are much lighter (29.6 ± 2.2 nm in parallel to AuNPs, Figure 1f). Janus-type PGPNs were also confirmed by scanning electron microscope (SEM, Figure 1c) in which the contrast is reversed. The UV−vis spectroscopy of Janus-type PGPNs and citrate-capped AuNPs are given in Figure 1d. The localized surface plasmon resonance (LSPR) peak is 529 and 520 nm for PGPNs and AuNPs, respectively. The sharp LSPR peak of PGPNs indicates the water solubility of Janus-type PGPNs. Janus-type PGPNs are stable in water and no obvious change was observed over three months. The average number of AuNPs per polymer domains (N_{Au}) analyzed statistically over 200 individual PGPNs from TEM is 0.95. The yield of Janus-type PGPNs is 91% without gradient centrifugation while around 9% of PGPNs have two polymer domains (Figure 1e).

The formation of Janus-type PGPNs was not observed without incubation overnight. Reducing the incubation time, like to less than 1 h, would result in the aggregation of AuNPs under annealing, as indicated by the color change from red to purple. This is presumably due to the lack of ligand protection. Our control experiments confirmed that both PS_{200}-SH and PAA_{107}-b-PS_{55} were critical to prepare high-quality Janus-type PGPNs. In the absence of PS_{200}-SH, similar purplish color was seen during annealing. Nanochain-like aggregates where AuNPs were linked by polymer micelles were observed under TEM (Figure S2). Without PAA_{107}-b-PS_{55}, PGPNs crushed out from the solution as large clusters of AuNPs after addition of water (Figure S2). Therefore, we deduce that the amphiphilic BCP of PAA_{107}-b-PS_{55} interacts with PS_{200}-SH grafted AuNPs upon the addition of water, driven by the hydrophobic interaction. The collapse of PS ligands on PGPNs, although destabilizing AuNPs in the DMF/water mixture, can be solubilized by PAA_{107}-b-PS_{55} acting as a surfactant.[19]

The formation of Janus-type PGPNs largely depends on $C_{PS200\text{-}SH}$. With $C_{PS200\text{-}SH}$ = 20.3−0.5 μM, there are clear morphological transitions of PGPNs from clustering to core−shell and eventually to Janus-type (see Figures S3−S8 with detailed statistics). At $C_{PS200\text{-}SH}$ = 20.3 μM, nanoclusters were observed under TEM (Figure 2a). The nanoclusters have a clear polymer outer shell with one or more AuNPs encapsulated. The size of nanoclusters is 51.2 ± 10.1 nm, and the N_{Au} is 1.9. When decreasing $C_{PS200\text{-}SH}$ to 5.1 μM, the N_{Au} shows a clear drop where 58% of PGPNs have individual AuNPs as the core. The average diameter decreases to 41.5 ± 8.3 nm. Further reducing $C_{PS200\text{-}SH}$ to 2.0 μM led to the formation of eccentric PGPNs (Figure 2c). Polymer domains mostly segregated to form asymmetric coating on AuNPs. The N_{Au} decreased to 1.15 with 86% of PGPNs having individual AuNPs per polymer domains (Figure 2g). Since polymer domains are not spherical, we defined the size of polymer

https://doi.org/10.1021/acsmacrolett.1c00252
ACS Macro Lett. 2021, 10, 786−790

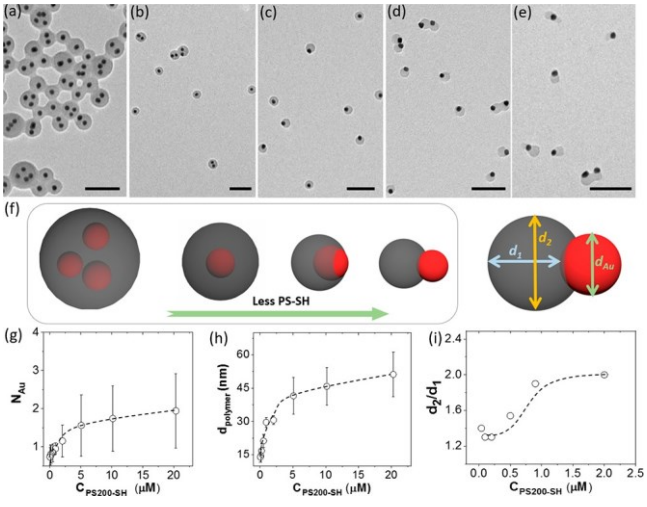

Figure 2. (a−e) TEM of PGPNs prepared with different $C_{PS200\text{-}SH}$ (μM): (a) 20.3; (b) 5.1; (c) 2.0; (d) 0.9; (e) 0.5. Scale bars are 100 nm. (f) Schemes showing morphological transitions of PGPNs by reducing $C_{PS\text{-}SH}$ (left) and definition of d_1 and d_2 of PGPNs (right). (g−i) Plotting N_{Au} (g), diameter of polymer domains (h), and d_2/d_1 (i) vs $C_{PS200\text{-}SH}$. $d_{polymer}$ is d_2 for Janus-type PGPNs.

domains in two different directions, that is, across (d_1) with and in parallel (d_2) to AuNPs (Figure 2f). The d_1 and d_2 are 14.8 ± 2.2 and 30.6 ± 2.0 nm, respectively, at $C_{PS200\text{-}SH}$ = 2.0 μM. At $C_{PS200\text{-}SH}$ in the range of 2.0 to 0.5 μM, Janus-type PGPNs were observed with N_{Au} close to 1 (Figures 2d,e and S6−S8), although the size of polymer domains varied with $C_{PS200\text{-}SH}$ (Figure 2h). When further decreasing $C_{PS200\text{-}SH}$ to 0.2 μM and below, the PGPNs were not stable in water where a new shoulder LSPR peak at 620 nm was observed (Figure S9). In those cases, PGPNs with two polymer domains were found similar to that without PS_{200}-SH (Figures S10−S12).

For Janus-type PGPNs, the surface coverage of AuNPs is controllable by varying $C_{PS200\text{-}SH}$. We used the ratio of d_2/d_1 that stands for the size difference of polymer domains at two different directions to quantify the surface coverage of AuNPs. A high ratio of d_2/d_1 is an indication of AuNPs presented close to the center of polymer domains, that is, a high coverage of AuNPs. Note that, since TEM only shows the 2D projection, the measured values of d_1 from TEM will be smaller than those of the real d_1. Although the statistical analysis (>200 NPs) would average out the difference among projection directions, it only provides semiquantitative comparison of the surface coverage. At $C_{PS200\text{-}SH} \geq 0.9$ μM, the d_2/d_1 of Janus-type PGPNs is 1.9−2 (Figure 2i and Table 1). The decrease of $C_{PS200\text{-}SH}$ led to the sharp drop of the d_2/d_1. At $C_{PS200\text{-}SH}$ = 0.2 μM, the d_2/d_1 is 1.3. Given the stability of PGPNs, the d_2/d_1 of 1.5−2 likely represents the optimal surface coverage of AuNPs to balance the phase segregation and their colloidal stability. The change in surface coverage of AuNPs further confirms our interpretation of deficient ligand coverage of AuNPs upon collapse.

We have quantitatively estimated the grafting density since the deficiency of PS_{200}-SH facilitates the structural transition of PGPNs. To do so, the BCP was selectively removed via thorough centrifugation cycles in pure DMF. Since PAA_{107}-b-PS_{55} is not chemically grafted on AuNPs, the residual polymers on PGPNs are presumably PS_{200}-SH. The grafting density was calculated through the shell thickness using TEM (Table S1). For $C_{PS200\text{-}SH}$ = 20.3 μM, the grafting density of AuNPs reached 0.41 per nm^2. The ligand density decreases linearly with $C_{PS200\text{-}SH}$ (Figures S13 and S14) at $C_{PS200\text{-}SH} \geq 5.1$ μM; therefore, under deficiency of ligands, the grafting of PS_{200}-SH on AuNPs follows a Langmuir adsorption model, where the ligand grafting is precisely controllable by decreasing $C_{PS200\text{-}SH}$. When Janus-type PGPNs are identified as the major products at $C_{PS200\text{-}SH}$ = 2.0 μM, the grafting density of ~0.1 per nm^2, calculated from a linear extrapolation, is the critical value to allow phase segregation.

Table 1. Structural Parameters of PGPNs Prepared with Different Concentrations of PS_{200}-SH

$C_{PS200\text{-}SH}$ (μM)	d_1 (nm)	d_2 (nm)	d_3 (nm)	d_2/d_1	stretching ratio[a]
20.3			44.0 ± 5.8		1.7
10.1			39.9 ± 3.6		1.4
5.1			35.7 ± 2.8		1.1
2.0	14.8 ± 2.2	30.6 ± 2.0	32.5 ± 2.2	2.0	0.9
0.9	15.4 ± 1.4	29.6 ± 2.2		1.9	
0.5	13.8 ± 2.1	21.2 ± 3.0		1.5	
0.2	12.5 ± 2.9	16.8 ± 3.2		1.3	
0.1	10.8 ± 2.0	14.5 ± 2.9		1.3	
0.04	9.9 ± 1.6	13.9 ± 2.3		1.4	

[a]Note: Stretching ratio for PS_{200}-SH.

Overall, hydrophobicity-driven collapsing of PS ligands results in an elongated chain conformation, as observed in densely packed hydrophobic cores of micelles.[20] We examined the grafting state of PS_{200}-SH at various grafting densities at $C_{PS200\text{-}SH} \geq 2.0$ μM. With a focus only on core−shell PGPNs with discrete AuNPs as the core, the diameter (d_3) of those core−shell PGPNs is dependent on $C_{PS200\text{-}SH}$ (Table 1). The difference in the size of core−shell PGPNs suggests that the chain stretching ratio (S) of hydrophobic PS_{200}-SH is varied among those core−shell PGPNs. If we consider the BCP chains that are fully relaxed as not being chemically bound to AuNPs, the decrease of d_3 is presumably due to the change in the chain stretching of PS_{200}-SH at different grafting densities.

The S of PS_{200}-SH can be calculated using

$$S = \frac{(d_3 - d_{Au})/2 - R_{0,PS\text{-}BCP}}{R_{0,PS_{200}\text{-}SH}}$$

where d_3 and d_{Au} are the diameter of core−shell PGPNs and AuNPs, respectively, and $R_{0,PS\text{-}BCP}$ and $R_{0,PS200\text{-}SH}$ are the root-mean-square end-to-end distance of PS in PAA_{107}-b-PS_{55} and PS_{200}-SH (Table S2), respectively. In all cases where clustering and core−shell PGPNs are the major products, the S is >1; therefore, polymer ligands are stretched to avoid the overlap with neighboring chains because of entropic repulsion. The phase segregation of ligands that will further increase the local grafting density cannot occur. The morphological transition from core−shell to Janus-type only occurred at $C_{PS200\text{-}SH}$ = 2.0 μM, with S ~ 0.9 (Table 1). With a low grafting density, the decrease of entropic repulsion among ligands makes the phase segregation possible. The transformation took place instead of further compressing PS_{200}-SH to maintain the low free energy of PGPNs. The asymmetric distribution of PS along the polar axis would minimize the interface of the solvent and PS_{200}-SH ligands where AuNPs protruded out of polymers and became exposed to solution.

The decrease of PS_{200}-SH resulted in the formation of spheroids. We approximated the shape transformation of PGPNs using a spheroid model to estimate the average volume

https://doi.org/10.1021/acsmacrolett.1c00252
ACS Macro Lett. 2021, 10, 786−790

(V_{PGPNs}) and surface area (S_{PGPNs}) per NP (see SI for details). In contrast to abrupted changes in the aspect ratio from sphere to spheroid, V_{PGPNs} and S_{PGPNs} undergo a continuous decrease with respect to $C_{PS200\text{-}SH}$ (Figure S15). It is interesting to note that V_{PGPN} and S_{PGPN} are correlated linearly, regardless of the final shapes of PGPNs. This suggests that the phase segregation occurs mainly to minimize the surface area of PGPNs with low density of PS-SH and avoid the energetic penalty in compressing polymer chains excessively.

To explore the controllability over the size of polymer domains, we examined PS-SH with different M_w (4.6 to 37 kg/mol). The same concentration of PS-SH (ca. 0.9 μM) was used while maintaining the concentrations of BCPs and AuNPs constant. Uniform Janus-type PGPNs with >90% yields of N_{Au} = 1 were seen for all PS-SH (Figures S16−S19). The size of polymer domains is dependent on the M_w of PS-SH (Figure 3a). With PS_{44}-SH, polymer domains are small, with a d_2 of

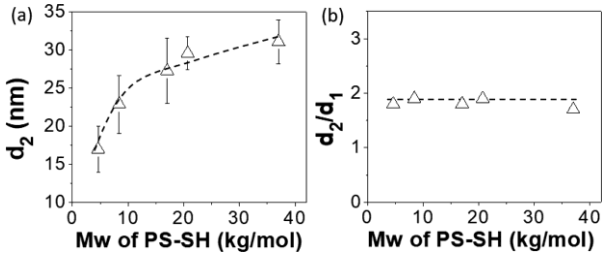

Figure 3. Plotting d_2 (a) and d_2/d_1 (b) of Janus-type PGPNs vs M_w of PS-SH.

17.4 ± 2.6 nm (Figure S17), while the d_2 increases to 31.1 ± 2.9 nm for PS_{356}-SH. Interestingly, the d_2/d_1 seems to be less sensitive to the M_w of PS-SH (Figure 3b). It is in the range of 1.9−1.7, regardless of the length of PS-SH. Those results confirm that the similar surface coverage of AuNPs can be achieved with a similar density of PS-SH during the DLE synthesis.

Janus-type PGPNs show distinct surface properties. The exposed surfaces of PGPNs not covered by polymers can be used as seeds to mediate the further growth of a second metal.[16b,21] Two proof-of-concept experiments were carried out to grow Au and Pd on Janus-type PGPNs prepared with $C_{PS200\text{-}SH}$ = 0.9 μM. For Au grown on Janus-type PGPNs (Au@Au), elongated Au domains with an average length of ~23 nm were seen on the only one side of the original Au cores (Figure 4a). The asymmetric growth of Au@Au resulted in a clear red-shift and broadening of the LSPR peak from 529 to 545 nm (Figure 4b), similar to the reported values of asymmetric Au@Au NPs.[21] A similar asymmetric growth was also seen for Pd@Au (Figure 4c). The new Pd domains are extruded on the exposed surface of AuNPs as confirmed by scanning TEM energy-dispersive X-ray spectroscopy (EDX) mapping (Figure S20). The LSPR peak of Pd@Au does not show a large shift but similar peak broadening as Au@Au.[16b,21,22] In both cases, no other capping agents are needed and the BCP surfactant can stabilize PGPNs during the secondary growth.

In summary, we demonstrated a facile synthetic approach to selectively pattern the surface of isotropic plasmonic AuNPs while undergoing ligand exchange with PS-SH. The concentration of PS-SH ligands played a central role in controlling the surface patterning of AuNPs while PAA-b-PS acted as a surfactant to stabilize PGPNs. With sufficient PS-SH ($C_{PS200\text{-}SH}$ ≥ 2 μM), AuNPs were coated isotopically with dense

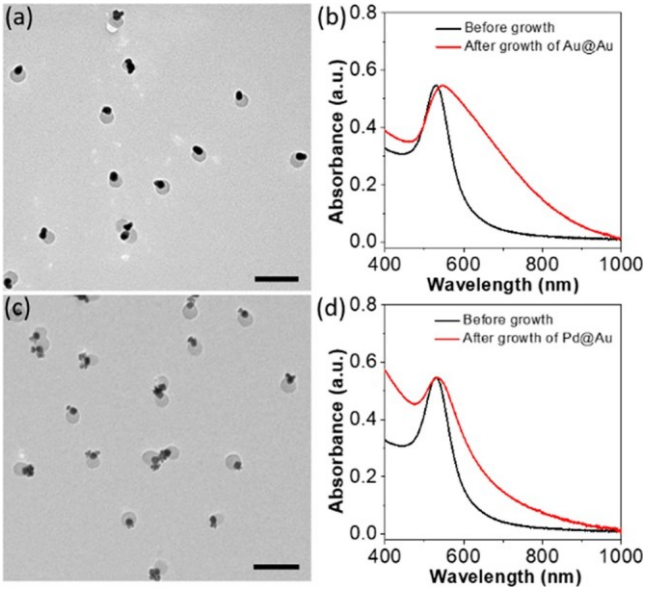

Figure 4. TEM and normalized UV−vis spectra of Au@Au (a, b) and Pd@Au (c, d) on Janus-type PGPNs. Scale bars are 100 nm in (a) and (c).

hydrophobic PS-SH ligands that further formed clusters or core−shell nanostructures in water. When the concentration of PS_{200}-SH was deficient (0.2 μM ≤ $C_{PS200\text{-}SH}$ ≤ 2.0 μM), Janus-type PGPNs were produced with selective surface coverage on AuNPs. The underlying mechanism of such structural transition was found to be the interplay of conformational entropy of PS-SH ligands and the interfacial energy between PGPNs and solvent. As-resultant core−shell or Janus-type PGPNs were stable in water and those could be produced in scale-up syntheses. Other synthetic parameters like the size of AuNPs and the hydrophobicity/block length of the BCP surfactant that potentially will lead to another level of controllability over the asymmetric patterning of polymer domains are currently undergoing. Our method is extremely simple to prepare high-quality symmetric-broken PGPNs with many potentials in hierarchical self-assembly and catalysis.

ASSOCIATED CONTENT

Supporting Information

The Supporting Information is available free of charge at https://pubs.acs.org/doi/10.1021/acsmacrolett.1c00252.

Detailed synthesis procedure, more electron microscope characterization, image analysis, grafting density, and UV−vis absorption spectroscopy (PDF)

AUTHOR INFORMATION

Corresponding Authors

Jie He − Polymer Program, Institute of Materials Science and Department of Chemistry, University of Connecticut, Storrs, Connecticut 06269, United States; orcid.org/0000-0003-0252-3094; Email: jie.he@uconn.edu

Yao Lin − Polymer Program, Institute of Materials Science and Department of Chemistry, University of Connecticut, Storrs, Connecticut 06269, United States; orcid.org/0000-0001-5227-2663; Email: yao.lin@uconn.edu

https://doi.org/10.1021/acsmacrolett.1c00252
ACS Macro Lett. 2021, 10, 786−790

Authors

Hanyi Duan − Polymer Program, Institute of Materials Science, University of Connecticut, Storrs, Connecticut 06269, United States

Qiang Luo − Department of Chemistry, University of Connecticut, Storrs, Connecticut 06269, United States

Zichao Wei − Department of Chemistry, University of Connecticut, Storrs, Connecticut 06269, United States; orcid.org/0000-0001-5818-5077

Complete contact information is available at: https://pubs.acs.org/10.1021/acsmacrolett.1c00252

Notes

The authors declare no competing financial interest.

ACKNOWLEDGMENTS

J.H. is grateful for the support from the ACS petroleum research foundation and the National Science Foundation (CBET-1705566). The SEM/TEM studies were performed using the facilities in the Bioscience Electron Microscopy Laboratory at the University of Connecticut (UConn) and UConn/Thermo Fisher Scientific Center for Advanced Microscopy and Materials Analysis (CAMMA).

REFERENCES

(1) (a) Liu, K.; Nie, Z.; Zhao, N.; Li, W.; Rubinstein, M.; Kumacheva, E. Science 2010, 327, 197−200. (b) Klinkova, A.; Choueiri, R. M.; Kumacheva, E. Chem. Soc. Rev. 2014, 43, 3976−3991. (c) Cutler, J. I.; Auyeung, E.; Mirkin, C. A. J. Am. Chem. Soc. 2012, 134, 1376−1391. (d) Kumar, S. K.; Jouault, N.; Benicewicz, B.; Neely, T. Macromolecules 2013, 46, 3199−3214. (e) Li, X.; Iocozzia, J.; Chen, Y.; Zhao, S.; Cui, X.; Wang, W.; Yu, H.; Lin, S.; Lin, Z. Angew. Chem., Int. Ed. 2018, 57, 2046−2070. (f) Yi, C.; Yang, Y.; Liu, B.; He, J.; Nie, Z. Chem. Soc. Rev. 2020, 49, 465−508. (g) Yi, C.; Liu, H.; Zhang, S.; Yang, Y.; Zhang, Y.; Lu, Z.; Kumacheva, E.; Nie, Z. Science 2020, 369, 1369−1374. (h) Duan, H.; Yang, Y.; Zhang, Y.; Yi, C.; Nie, Z.; He, J. Giant 2020, 4, 100033.

(2) (a) Li, Z.; Wang, W.; Yin, Y. Trends in Chemistry 2020, 2, 593. (b) Nie, Z.; Fava, D.; Kumacheva, E.; Zou, S.; Walker, G. C.; Rubinstein, M. Nat. Mater. 2007, 6, 609−614. (c) Jones, S. T.; Walsh-Korb, Z.; Barrow, S. J.; Henderson, S. L. del Barrio, J.; Scherman, O. A. ACS Nano 2018, 10, 9156−9165. (d) Sánchez-Iglesias, A.; et al. ACS Nano 2012, 6, 11059−11065. (e) Grzelczak, M.; Sánchez-Iglesias, A.; Mezerji, H. H.; Bals, S.; Pérez-Juste, J.; Liz-Marzán, L. M. Nano Lett. 2012, 12, 4380−4384. (f) Liu, K.; Lukach, A.; Sugikawa, K.; Chung, S.; Vickery, J.; Thérien-Aubin, H.; Yang, B.; Rubinstein, M.; Kumacheva, E. Angew. Chem., Int. Ed. 2014, 53, 2648−2653. (g) Han, X.; Liu, Y.; Yin, Y. Nano Lett. 2014, 14, 2466−2470. (h) Liu, L.; Gao, Z.; Jiang, B.; Bai, Y.; Wang, W.; Yin, Y. Nano Lett. 2018, 18, 5312−5318.

(3) Song, J.; Cheng, L.; Liu, A.; Yin, J.; Kuang, M.; Duan, H. J. Am. Chem. Soc. 2011, 133, 10760−10763.

(4) (a) Nie, Z.; Xu, S.; Seo, M.; Lewis, P. C.; Kumacheva, E. J. Am. Chem. Soc. 2005, 127, 8058−8063. (b) He, J.; Liu, T.; Babu, T.; Wei, Z.; Nie, Z. J. Am. Chem. Soc. 2012, 134, 11342−11345. (c) Luo, Q.; Hickey, R. J.; Park, S.-J. ACS Macro Lett. 2013, 2, 107−111. (d) Hickey, R. J.; Haynes, A. S.; Kikkawa, J. M.; Park, S.-J. J. Am. Chem. Soc. 2011, 133, 1517−1525. (e) Wang, H.; Chen, L.; Shen, X.; Zhu, L.; He, J.; Chen, H. Angew. Chem., Int. Ed. 2012, 51, 8021−8025. (f) Wang, Y.; et al. Nat. Commun. 2010, 1, 87. (g) Chen, G.; Wang, Y.; Yang, M.; Xu, J.; Goh, S. J.; Pan, M.; Chen, H. J. Am. Chem. Soc. 2010, 132, 3644−3645. (h) Ma, S.; Hu, Y.; Wang, R. Macromolecules 2016, 49, 3535−3541. (i) Ma, S.; Qi, D.; Xiao, M.; Wang, R. Soft Matter 2014, 10, 9090−9097. (j) Lee, H.-Y.; Shin, S. H. R.; Drews, A. M.; Chirsan, A. M.; Lewis, S. A.; Bishop, K. J. M. ACS Nano 2014, 8, 9979−9987. (k) Li, R.; et al. J. Am. Chem. Soc. 2019, 141, 19542−19545.

(5) (a) Yang, K.; Zhang, S.; He, J.; Nie, Z. Nano Today 2021, 36, 101046. (b) He, J.; et al. J. Am. Chem. Soc. 2013, 135, 7974−7984. (c) Alhasan, A. H.; Patel, P. C.; Choi, C. H. J.; Mirkin, C. A. Small 2014, 10, 186−192. (d) Song, J.; et al. J. Am. Chem. Soc. 2019, 141, 8158−8170. (e) McQuade, C.; et al. Small 2015, 11, 834−843. (f) Song, J.; Zhou, J.; Duan, H. J. Am. Chem. Soc. 2012, 134, 13458−13469.

(6) (a) Uehara, N. Anal. Sci. 2010, 26, 1219−1228. (b) Moyano, D. F.; Rana, S.; Bunz, U. H.; Rotello, V. M. Faraday Discuss. 2011, 152, 33−42. (c) Sánchez-Iglesias, A.; Claes, N.; Solís, D. M.; Taboada, J. M.; Bals, S.; Liz-Marzán, L. M.; Grzelczak, M. Angew. Chem. 2018, 130, 3237−3240.

(7) (a) Zhang, L.; Wei, Z.; Thanneeru, S.; Meng, M.; Kruzyk, M.; Ung, G.; Liu, B.; He, J. Angew. Chem. 2019, 131, 15981−15987; (b) Zhang, L.; Wei, Z.; Meng, M.; Ung, G.; He, J. J. Mater. Chem. A 2020, 8, 15900−15908. (c) Pan, S.; He, L.; Peng, J.; Qiu, F.; Lin, Z. Angew. Chem. 2016, 128, 8828−8832.

(8) (a) Gröschel, A. H.; Walther, A.; Löbling, T. I.; Schacher, F. H.; Schmalz, H.; Müller, A. H. Nature 2013, 503, 247−251. (b) Choueiri, R. M.; et al. Nature 2016, 538, 79−83. (c) Yi, C.; Yang, Y.; Nie, Z. J. Am. Chem. Soc. 2019, 141, 7917−7925.

(9) Glotzer, S. C.; Solomon, M. J. Nat. Mater. 2007, 6, 557−562.

(10) (a) Wang, B.; Li, B.; Zhao, B.; Li, C. Y. J. Am. Chem. Soc. 2008, 130, 11594−11595. (b) Kim, A.; Zhou, S.; Yao, L.; Ni, S.; Luo, B.; Sing, C. E.; Chen, Q. J. Am. Chem. Soc. 2019, 141, 11796−11800. (c) Choueiri, R. M.; Klinkova, A.; Thérien-Aubin, H.; Rodriguez-Rodriguez, M.; Kumacheva, E. J. Am. Chem. Soc. 2013, 135, 10262−10265.

(11) Hinman, J. G.; Eller, J. R.; Lin, W.; Li, J.; Li, J.; Murphy, C. J. J. Am. Chem. Soc. 2017, 139, 9851−9854.

(12) Gao, B.; Arya, G.; Tao, A. R. Nat. Nanotechnol. 2012, 7, 433−437.

(13) (a) Lee, H.-Y.; Shin, S. H. R.; Abezgauz, L. L.; Lewis, S. A.; Chirsan, A. M.; Danino, D. D.; Bishop, K. J. M. J. Am. Chem. Soc. 2013, 135, 5950−5953. (b) Chen, G.; et al. Nat. Mater. 2019, 18, 169−174. (c) Chen, T.; Chen, G.; Xing, S.; Wu, T.; Chen, H. Chem. Mater. 2010, 22, 3826−3828. (d) Singh, C.; Ghorai, P. K.; Horsch, M. A.; Jackson, A. M.; Larson, R. G.; Stellacci, F.; Glotzer, S. C. Phys. Rev. Lett. 2007, 99, 226106.

(14) Chen, T.; Yang, M.; Wang, X.; Tan, L. H.; Chen, H. J. Am. Chem. Soc. 2008, 130, 11858−11859.

(15) DeVries, G. A.; Brunnbauer, M.; Hu, Y.; Jackson, A. M.; Long, B.; Neltner, B. T.; Uzun, O.; Wunsch, B. H.; Stellacci, F. Science 2007, 315, 358−361.

(16) (a) Galati, E.; Tao, H.; Rossner, C.; Zhulina, E. B.; Kumacheva, E.; Lopes, A.; Jin, L.; McCabe, M.; He, J. Small 2017, 13, 1700091.

(17) Yang, Y.; Yi, C.; Duan, X.; Wu, Q.; Zhang, Y.; Tao, J.; Dong, W.; Nie, Z. J. Am. Chem. Soc. 2021, 143, 5060−5070.

(18) (a) Kim, A.; Yao, L.; Kalutantirige, F.; Zhou, S.; Chen, Q. Patchy Nanoparticle Synthesis and Self-Assembly. Self-Assembly of Nanostructures; IntechOpen, 2020. (b) Hu, H.; et al. ACS Nano 2016, 10, 7323−7330. (c) Wang, Y.; Wang, Y.; Breed, D. R.; Manoharan, V. N.; Feng, L.; Hollingsworth, A. D.; Weck, M.; Pine, D. J. Nature 2012, 491, 51−55.

(19) Zhang, L.; Eisenberg, A. J. Am. Chem. Soc. 1996, 118, 3168−3181.

(20) Won, Y. Y.; Bates, F. S. Nonionic block copolymer wormlike micelles. Giant Micelles: Properties and Applications; CRC Press, 2007; pp 417−452.

(21) Qiu, J.; Xie, M.; Lyu, Z.; Gilroy, K. D.; Liu, H.; Xia, Y. Nano Lett. 2019, 19, 6703−6708.

(22) (a) Logsdail, A. J.; Johnston, R. L. J. Phys. Chem. C 2012, 116, 23616−23628. (b) Zhu, C.; Zeng, J.; Tao, J.; Johnson, M. C.; Schmidt-Krey, I.; Blumwald, E.; Zhu, Y.; Gu, Z.; Xia, Y. J. Am. Chem. Soc. 2012, 134, 13822−13834.